Research Article Vol. 30, No. 26 / 19 Dec 2022 / Optics Express 47315
Optics EXPRESS

Comparative study of medium length-dependent high-harmonic generation from metal ions

WUFENG FU,[1,2] YU HANG LAI,[1,3,4] AND WEI LI[1,2,5]

[1]GPL Photonics Laboratory, State Key Laboratory of Applied Optics, Changchun Institute of Optics, Fine Mechanics and Physics, Chinese Academy of Sciences, Changchun 130033, China
[2]University of Chinese Academy of Sciences, Beijing 100049, China
[3]Department of Physics, The Chinese University of Hong Kong, Hong Kong SAR, China
[4]yuhanglai@cuhk.edu.hk
[5]weili1@ciomp.ac.cn

Abstract: We present an experimental study on the high-harmonic yields from the ions in the laser-ablated plumes of various metal targets (W, Mo, Cr, Cu, Ni, Fe, Ag and Mg) with the purpose of comparing their ion density and single-atom response. The harmonic yields as a function of medium length are measured and the results are fitted against a theoretical model to extract the coherence length, absorption length and strength single-atom response (in arbitrary units) of different harmonic orders for each target. It is found that the coherence lengths decrease monotonically as a function of harmonic order for all targets. Ion density of the generation media are estimated by the trend of the coherence length as a function of harmonic order. Qualitatively, targets with lower melting temperatures seem to produce laser-ablated plumes of higher ion density, vice versa. Also, the strength of the single-atom response of the metal ion species with only one electron in the outermost subshell are weak compared with the other targets considered in this study.

1. Introduction

High-harmonic generation (HHG) is one of the most important phenomena in strong-field atomic physics. It can be used to generate ultrashort, coherent extreme ultraviolet pulses [1,2] and has become an attractive tool in ultrafast science [3,4].

In atomic HHG, noble gases have been the most common choices for the generation medium, as they are easy to handle (simply by using gas jets or gas cells) and can withstand high driving laser intensity [5–7]. Using metal atoms in vapor form are much less convenient due to the demanding requirement of heating. In fact, HHG in metal vapors have been demonstrated only for alkali atoms which are easy to be vaporized such as Cs [8] and Rb [9]. Fortunately, laser ablation may be treated as a convenient alternative to effusive atomic beam [10,11] for the purpose of HHG. By focusing an intense laser pulse on a metal surface, a plasma plume containing metal atoms and ions with sufficient density can be readily formed [12]. This method drastically widens the choices of atom species for HHG as it is effective for most metals regardless of their thermal properties.

So far, more than twenty kinds of metals have been used to produce laser-ablated plasma plumes (LPPs) for HHG [13–16] and there are several techniques [17,18] to enhance the yield and stability of harmonics [19]. Significant variations in cut-off energy [20,21] and harmonic yield among different metal species [22,23] have been observed but the reasons are still not very clear. In particular, quantifying and understanding the difference in harmonic yield is not straightforward since the yield does not only depend on the single-atomic response of the target, but also the macroscopic properties of the medium which affect phase matching and absorption effects [5,24–27]. Moreover, unlike gaseous medium whose density can be adjusted and monitored rather precisely without much effort, the density of ions in LPPs are very difficult,

#475483 https://doi.org/10.1364/OE.475483
Journal © 2022 Received 19 Sep 2022; revised 26 Oct 2022; accepted 13 Nov 2022; published 13 Dec 2022

Optics EXPRESS

if not impractical, to control and measure precisely. This causes another major difficulty in performing systematic comparison on HHG from different target species as the difference in ion density in different targets is hardly trackable.

In this work, we attempt to separate the effect of single-atom response from the macroscopic effect in order to obtain a relative comparison of the strength of single-atom response between eight different metal targets (W, Mo, Cr, Cu, Ni, Fe, Ag and Mg). These targets are selected in order to cover a wide range of harmonic cutoff. The goal is achieved by measuring the medium length L_{med} dependence of harmonics yields, which vary like a damped cosine function due to the macroscopic effect of phase matching and absorption. Then the experimental yields are fitted against the theoretical formula derived by E. Constant et al. [24] which describes how high-harmonic yields depend on the strength of single-atom response, coherence length and absorption length of the medium. Note that the first quantity describes the property of individual atom, and the last two quantities reflect the macroscopic properties of the medium. By treating these three quantities as the fitting parameters, we obtain the strength of single-atom response (in arbitrary units) for all the targets in this study. In addition, the fitted values of coherence length could also be used to estimate the ion density of the laser-ablated plumes from the metals [28].

2. Experimental setup

In this experiment, a commercial Ti: sapphire chirped pulsed amplifier system (Spectra Physics: Sprifire Ace) with a center wavelength of 0.8 μm and a repetition rate of 1000 Hz is used. Before temporal compression, the amplified laser beam in the system is split into two. One of them is sent out of the laser system without compression (pulse duration = 210 ps); it is the heating pulse (HP) which is used to generate LPP from the metal sample surface. The other beam, which is temporally compressed to 35 fs, is the driving pulse (DP) for generating high harmonics in the LPP. A significantly longer optical path is built for the DP such that it is temporally delayed by ~50 ns relative to the HP. The delay is fixed throughout the entire study for all targets.

The optical setup for HHG is schematically shown in Fig. 1. The HP is first focused by a cylindrical lens with a focal length of 200 mm. It is then imaged onto the metal sample surface by a 2:1 telescope. An adjustable slit is placed at the focal plane of the cylindrical lens to truncate the line focused laser beam. By adjusting the slit width, the length of HP on the sample surface, thus the length of the LPP, can be precisely controlled [29].The HP intensity at the sample surface is estimated to be about 15 GW/cm^2. On the other hand, the DP, with a maximum estimated

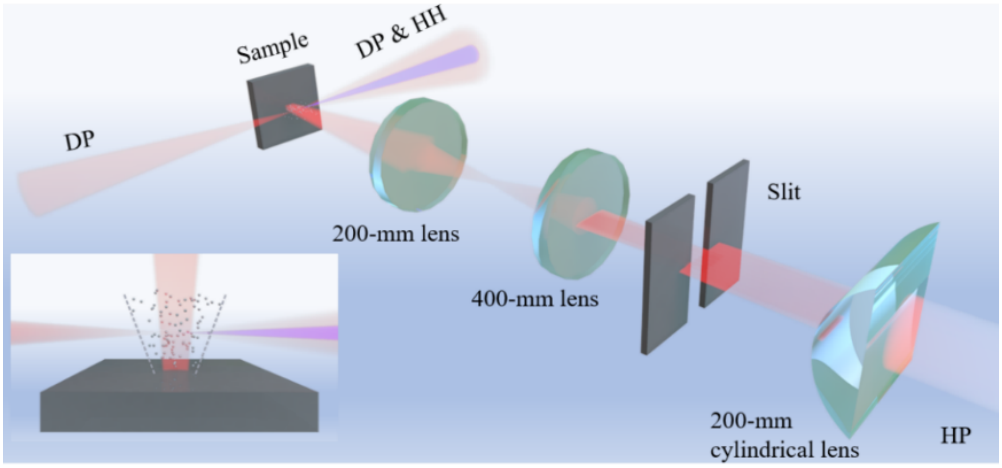

Fig. 1. Schematic diagram of the experimental setup.

Optics EXPRESS

intensity of 240 TW/cm^2, is focused by a convex lens and propagates parallel to the sample face. The ions in the LPP are driven by the DP and the generated high-harmonics are measured by a home-built spectrometer consisting of an entrance slit, a concave mirror, a 1200 grooves/mm flat field grating, a microchannel plate with a fluorescent screen and a CCD camera. Each raw harmonic spectrum is the accumulated result of a certain number of laser shots. Then, the spectral intensity is divided by the number of laser shots. That is, each presented harmonic spectrum below represents the averaged harmonic signal detected per laser shot.

3. Results and discussion

High-harmonic spectra at various length of LPP medium are measured for all the selected metal species in this study. As an example, Fig. 2 shows the results for Cu. More than 20 spectra at different medium length ranged between 0.2 and 1.4 mm are stacked together and presented all together as the false color map in Fig. 2(a). To display the variation more clearly, spectra at three of the medium length values (0.3, 0.5 and 0.7 mm) are shown in Fig. 2(b). We extract yield of each harmonic order as a function of medium length. The results for three of the harmonic orders (25th, 31st and 37th) are displayed in Fig. 2(c).

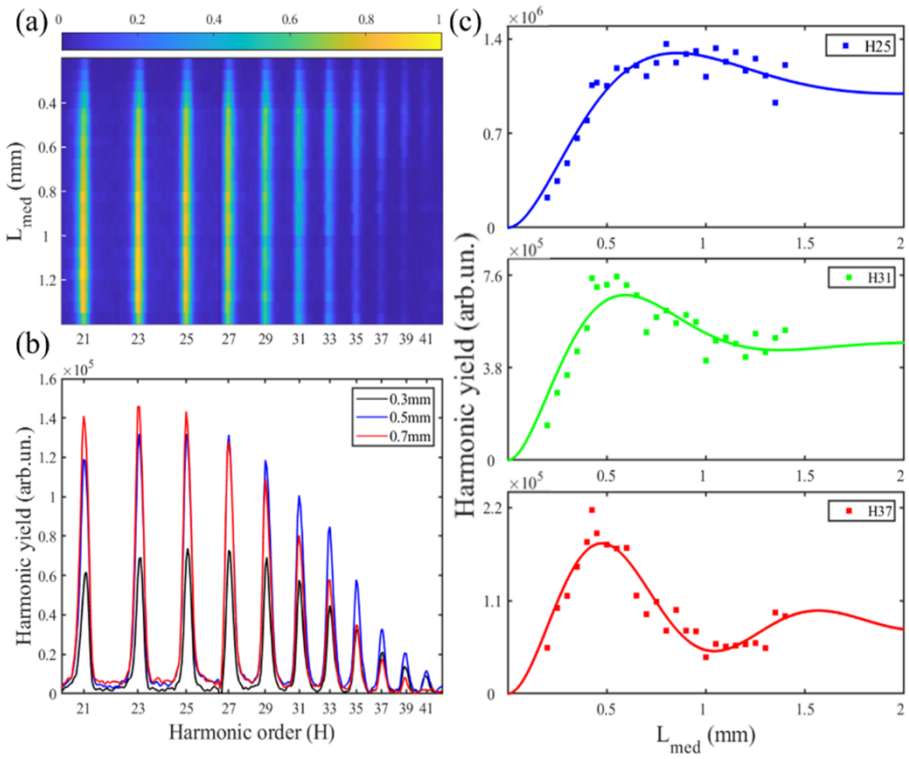

Fig. 2. HHG in plasma plume of Cu. (a) Harmonic spectra as a function of medium length. (b) Harmonic spectra at three of the medium lengths: 0.3mm, 0.5mm, 0.7mm. (c) The harmonic yields as a function of medium length for three of the harmonic orders: 25th, 31st and 37th. The dots are the data from the experiments. The lines are obtained by fitting experimental data according to Eq. (1).

Optics EXPRESS

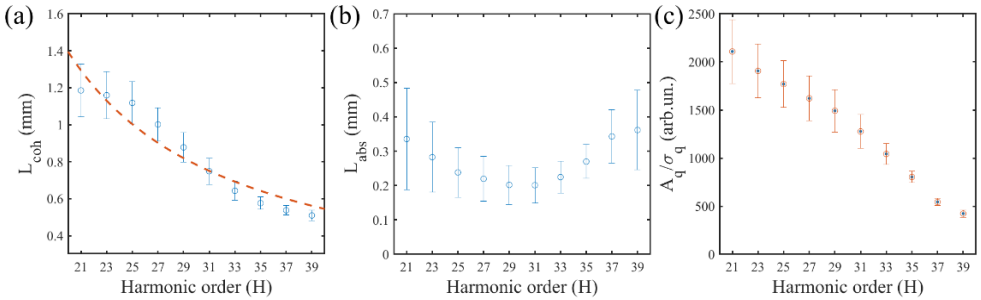

Fig. 3. According to Eq. (1), the fitted parameters of Cu from Fig. 2. (a) L_{coh} (b) L_{abs} and (c) A_q/σ_q. The dots are the parameters, the error bars are the 95% confidence limits and the dash line in Fig. 3(a) is fitted by $L_{coh} = \pi/(a_1 q + a_2)$.

According to E. Constant et al. [24], the medium length L_{med} dependence of the number of emitted q^{th} harmonic photons N_{out} on axis per unit length is given by

$$N_{out} \propto \frac{4q\omega(A_q/\sigma_q)^2}{1+4\pi^2\,(L_{abs}/L_{coh})^2}[1+\exp(-\frac{L_{med}}{L_{abs}})-2\cos(\frac{\pi L_{med}}{L_{coh}})\exp(-\frac{L_{med}}{2L_{abs}})] \tag{1}$$

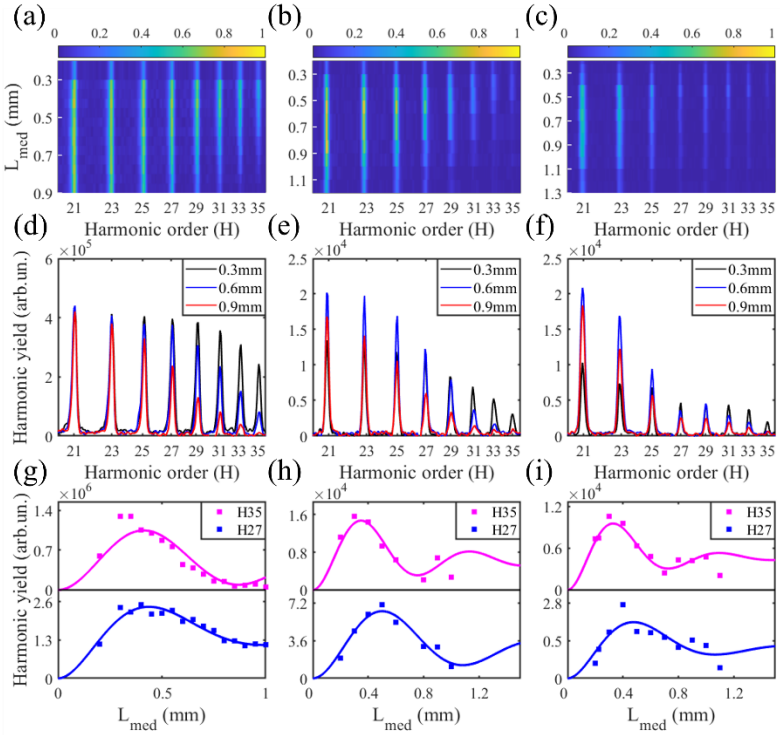

Fig. 4. Results of HHG from with the targets with relatively high harmonic cut-off energies. Harmonic spectra as a function of medium length for (a) Ag, (b) Ni, (c) W. Harmonic spectra at three different selected medium lengths for (d) Ag, (e) Ni, (f) W. The harmonic yields as a function of medium length for two of the harmonic orders for (g) Ag, (h) Ni, (i) W. The dots are the data from the experiments. The lines are obtained by fitting experimental data according to Eq. (1).

Optics EXPRESS

where ω is the laser angular frequency, L_{coh} is the coherence length of the medium, L_{abs} is the absorption length of the medium, A_q is single-atom response of q^{th} harmonic photons and σ_q is the single-atom absorption cross section of q^{th} harmonic photon. In the asymptotic limit $L_{med} \to \infty$, the harmonic intensity is proportional to the squared value of the ratio A_q/σ_q. That is, the ratio determines the so-called absorption limited conversion efficiency [24]. Note that L_{coh} and the phase-mismatch Δk in harmonic generation is related by $L_{coh} = \pi/\Delta k$. The formula indicates that harmonic intensity does not increase indefinitely as a function of medium length due to reabsorption by the medium itself. Moreover, due to phase-mismatch, N_{out} decreases when L_{med} is increased beyond L_{coh}. However, complete disappearance of harmonic signal does not occur in practice as the absorption causes imperfect destructive interference.

Treating L_{coh}, L_{abs} and A_q/σ_q as the fitting parameters, the data of harmonic yields for different order are fitted to Eq. (1). For instance, the fitted curves for the data of the 25$^{\text{th}}$, 31$^{\text{st}}$ and 37$^{\text{th}}$ order are shown by the solid lines in Fig. 2(c). Note that a shorter period of the cosine-like variation implies a shorter coherence length, vice versa. The fitted values of L_{coh}, L_{abs} and A_q/σ_q

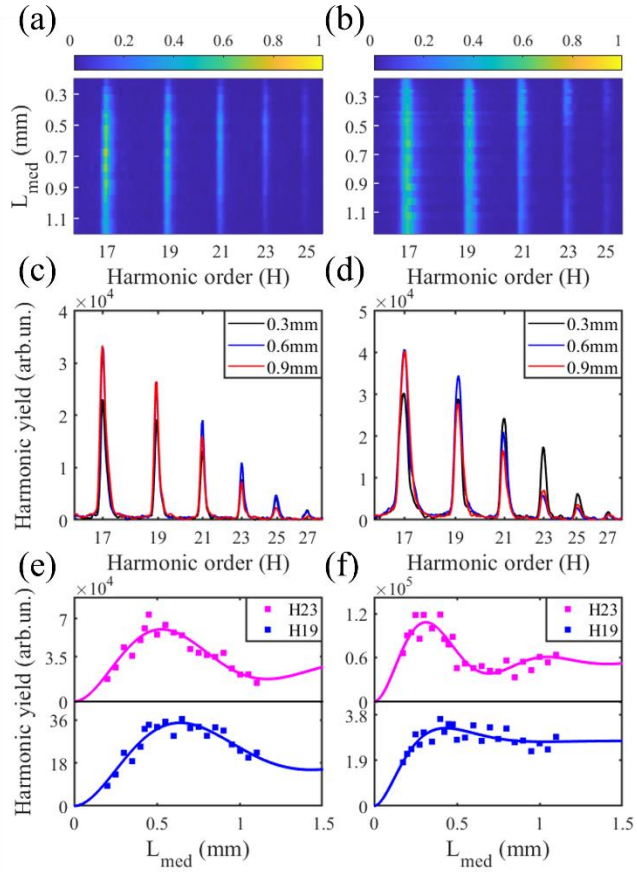

Fig. 5. Results of HHG from the targets with relatively lower harmonic cut-off energies. Harmonic spectra as a function of medium length for (a) Fe, (b) Mg. Harmonic spectra at three different selected medium lengths for (c) Fe, (d) Mg. The harmonic yields as a function of medium length for two of the harmonic orders for (e) Fe, (f) Mg. The dots are the data from the experiments. The lines are obtained by fitting experimental data according to Eq. (1).

Optics EXPRESS

for different harmonic orders are shown in Fig. 3(a)-(c), respectively. The decreasing trend of L_{coh} as a function of harmonic order can be understood by the general properties of phase-matching. In HHG, the four main factors that contribute to phase-mismatch are the neutral-atom dispersion, the plasma dispersion, the laser Gouy phase and the intensity-dependent phase [28,30,31]:

$$\begin{aligned}\Delta k &= \Delta k_{atom} + \Delta k_{plasma} + \Delta k_{Guoy} + \Delta k_{IDP} \\ &\approx \frac{q\omega_0}{c}(n_q - n_0) + \frac{q\rho_e e^2}{2m_e\varepsilon_0\omega_0 c} + \frac{b(q-1)}{b^2+4z^2} + \Delta k_{IDP}\end{aligned} \tag{2}$$

where q is the harmonic order, ω_0 is the frequency of the DP, n_q and n_0 are the refractive indices of the neutral atomic medium at the frequency of the q^{th} order harmonic and the DP, respectively, ρ_e is the free-electron density, and b is the confocal parameter. As shown, the first three terms are approximately proportional to q. In other words, the dependence of L_{coh} on q can be approximately expressed as $L_{coh} = \pi/(a_1 q + a_2)$ for some a_1 and a_2. The data points of L_{coh} are fitted to this equation with a_1 and a_2 being the fitting parameter. The fitted curve is presented by the dashed line in Fig. 3(a).

Assuming plasma dispersion is the most significant term among the first three terms, as suggested in Ref. [29], the fitted value of a_1 can be used to estimate the plasma density ρ_e since $a_1 = \rho_e e^2/(2m_e\varepsilon_0\omega_0 c)$. With this method, the plasma density, thus the ion density, in the LPP of

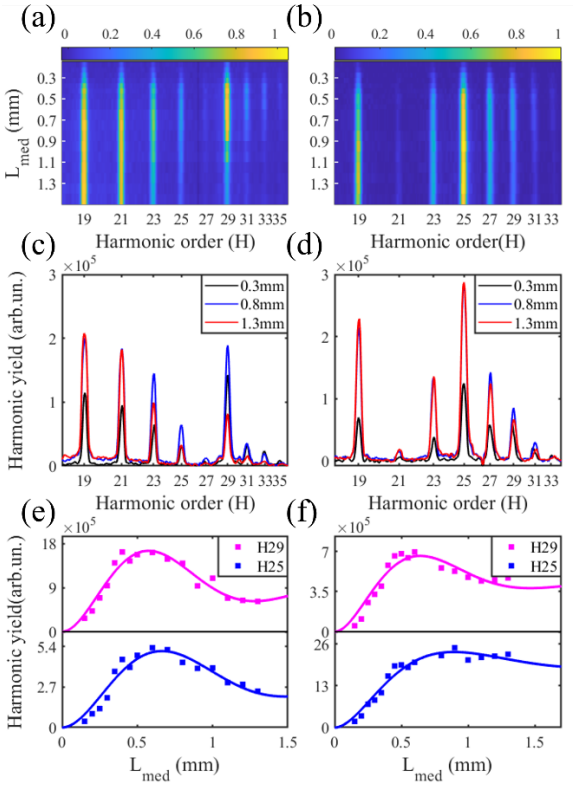

Fig. 6. Results of HHG from the targets with resonance enhancement features. Harmonic spectra as a function of medium length: (a) Cr, (b) Mo. Harmonic spectra at three selected medium lengths: (c) Cr, (d) Mo. The harmonic yields as a function of medium length for two of the harmonic orders: (e) Cr, (f) Mo. The dots are the data from the experiments. The lines are obtained by fitting experimental data according to Eq. (1).

Optics EXPRESS

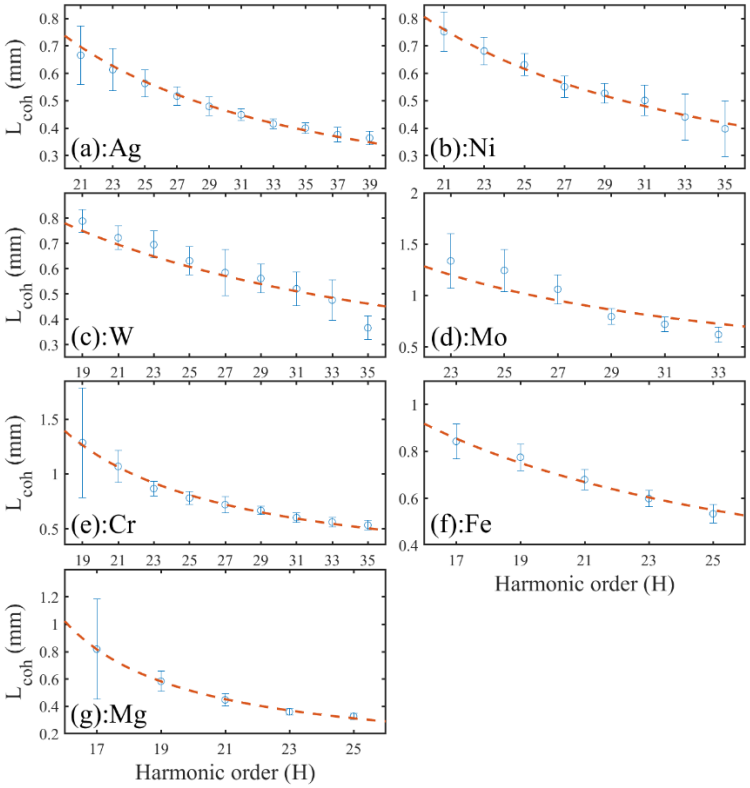

Fig. 7. L_{coh} as a function of the harmonic order for the metal of (a) Ag, (b) Ni, (c) W, (d) Mo, (e) Cr, (f) Fe and (g) Mg. The dots are L_{coh} deduced from Figs. 4–6, the error bars are the 95% confidence limits, and the dash lines are fitted by $L_{coh} = \pi/(a_1 q + a_2)$.

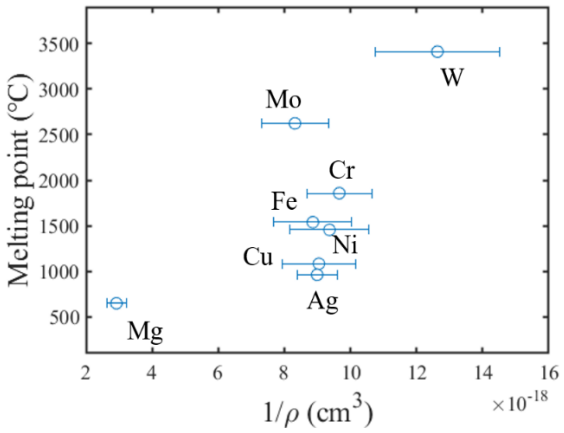

Fig. 8. The plot of melting point of the metal against the inverse of ion density. The ion density is estimated from a_1, which is derived from Fig. 3(a) and Fig. 7.

Cu is estimated to be $1.1 \times 10^{17}/\text{cm}^3$. The other two fitted parameters, L_{abs} and A_q/σ_q, are shown in Fig. 3(b) and (c), respectively.

Optics EXPRESS

The same measurement and fitting procedures are applied for the other eight metal targets, and the spectra are presented in Fig. 4 (for Ag, Ni and W), Fig. 5 (for Fe and Mg), and Fig. 6 (for Cr and Mo). In each figure, the false color maps in the top column shows the raw spectra at all L_{med}; the middle column shows the spectra at three selected L_{med}; and the bottom column shows the dependence of harmonic yield on L_{med} for two of the selected harmonic orders.

The three metal targets presented in Fig. 4 (Ag, Ni and W), and the Cu shown in Fig. 2, are the ones with relatively high harmonic cut-off energies. On the other hand, Fe and Mg in Fig. 5 have lower cut-off energies. As for Fig. 6, Cr and Mo are two interesting targets exhibited resonance features which have been investigated extensively [14,29,32,33]. For an investigation on comparing the harmonic cut-off between different targets, the readers may refer to a recent publication by the authors [34]. Note that the harmonic cut-offs of some targets shown in this work appear to be slightly lower than that presented in [34]. It is just because in this experiment we need to avoid saturation of pixels in our CCD camera for majority of the harmonic orders, and therefore we have to keep the overall harmonic signal moderate at the expense of the visibility of the highest few orders close to the cut-off.

As mentioned, the fitting procedures for Cu are applied for all the other targets. The fitted values of L_{coh} as a function of harmonic orders for them are shown in Fig. 7(a)–(h), respectively. Similar to Fig. 3(a), the dashed lines are the fitted curves in the form of $L_{coh} = \pi/(a_1 q + a_2)$ for estimating plasma density from the trend of L_{coh}. The estimated ion density for all targets are summarized in Fig. 8. It is a plot of melting point of the metal against the inverse of plasma density. Note that the specific heat capacities of these metals are very similar to each other. Although the process of forming plasma plume from a solid metal by laser ablation is vastly different from simply heating a solid metal from solid to gaseous form [35,36], it is not unreasonable to expect that, given a fixed amount of energy deposited into the material, the amount of matter in the ablated plume is larger for material with lower melting point, vice versa. Such a trend can be seen in Fig. 8 qualitatively. That is, the melting point increases with the inverse of ion density.

Finally, we present the comparison of A_q/σ_q between different targets in Fig. 9. Each panel shows the comparison for one harmonic order only. The results from the 21st harmonic up to the 31st harmonic are presented. Note that it is very likely that the measured harmonic spectra are mostly contributed by ions rather than neutral atoms. It is because the neutral atoms of metals have very low ionization potentials and so could only withstand very low driving laser intensity [34]. In other words, the results reflect the A_q/σ_q values of ions rather than neutral atoms. Also, note that the particularly low A_q/σ_q value of Mo at the 21st order, which is not shown in Fig. 9(a) and the high A_q/σ_q value of Cr at the 29th order are due to resonance effects [32,33].

Identifying the physical origin of the differences requires in-depth theoretical investigation and is beyond the scope of this work. Qualitatively, it seems that the targets with only one electron in the outermost subshell (Mg^+, W^+ and Fe^+) tends to have weaker response.

Optics EXPRESS

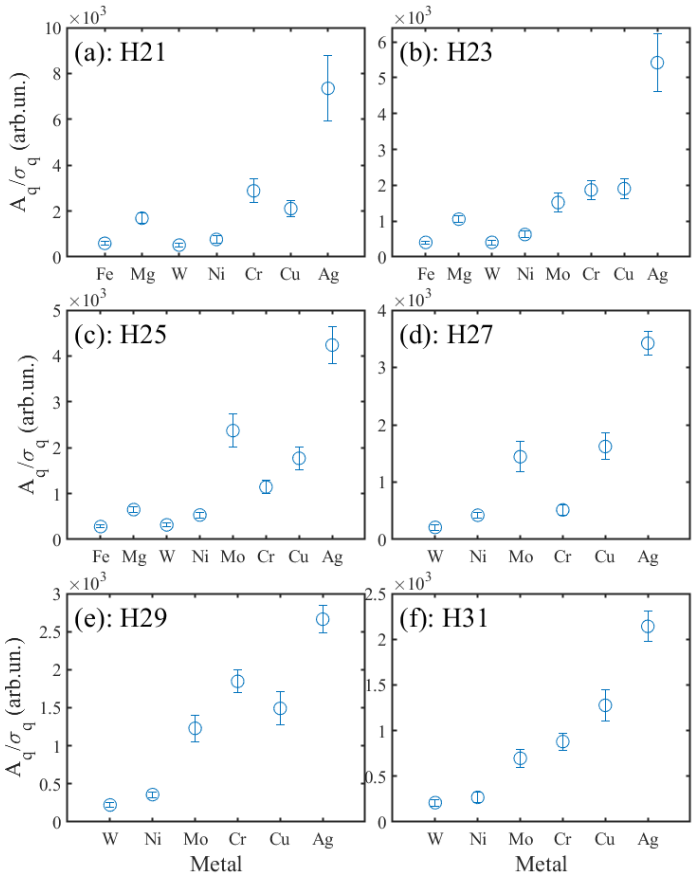

Fig. 9. A_q/σ_q of the different metals for harmonic order: (a) H21, (b) H23, (c) H25, (d) H27, (e) H29, (f) H31.

4. Conclusion

In summary, we measured the harmonic spectra from LPPs of eight different metals as a function of the medium length. Using the theoretical formula derived by E. Constant et al. [24], we extracted the three parameters: L_{coh}, L_{abs} and A_q/σ_q for every targets. From L_{coh}, we estimated the ion density of each target and found that the plasma density depends to the melting point of metal materials. We also found that the single-atom response of the metal ion species with only one electron in the outermost subshell are weak compared with the other targets considered in this study.

Funding. National Natural Science Foundation of China (12004380, 62121005); Innovation Grant of Changchun Institute of Optics, Fine Mechanics and Physics; Jilin Provincial Science & Technology Development Project (YDZJ202102CXJD002); Development Program of the Science and Technology of Jilin Province (20200802001GH).

Disclosures. The authors declare no competing financial interest.

Data availability. Data underlying the results presented in this paper are not publicly available at this time but may be obtained from the authors upon reasonable request.

References

1. T. Popmintchev, M.-C. Chen, D. Popmintchev, P. Arpin, S. Brown, S. Ališauskas, G. Andriukaitis, T. Balčiunas, O. D. Mücke, A. Pugzlys, A. Baltuška, B. Shim, S. E. Schrauth, A. Gaeta, C. Hernández-García, L. Plaja, A. Becker, A. Jaron-Becker, M. M. Murnane, and H. C. Kapteyn, "Bright Coherent Ultrahigh Harmonics in the keV X-ray Regime from Mid-Infrared Femtosecond Lasers," Science **336**(6086), 1287–1291 (2012).

Optics EXPRESS

2. T. Gaumnitz, A. Jain, Y. Pertot, M. Huppert, I. Jordan, F. Ardana-Lamas, and H. J. Wörner, "Streaking of 43-attosecond soft-X-ray pulses generated by a passively CEP-stable mid-infrared driver," Opt. Express **25**(22), 27506–27518 (2017).
3. K. Klünder, J. M. Dahlstrom, M. Gisselbrecht, T. Fordell, M. Swoboda, D. Guenot, P. Johnsson, J. Caillat, J. Mauritsson, A. Maquet, R. Taieb, and A. L'Huillier, "Probing Single-Photon Ionization on the Attosecond Time Scale," Phys. Rev. Lett. **106**(14), 143002 (2011).
4. L. He, S. Sun, P. Lan, Y. He, B. Wang, P. Wang, X. Zhu, L. Li, W. Cao, P. Lu, and C. D. Lin, "Filming movies of attosecond charge migration in single molecules with high harmonic spectroscopy," Nat. Commun. **13**(1), 4595–4603 (2022).
5. D. Popmintchev, C. Hernández-García, F. Dollar, C. Mancuso, J. Pérez-Hernández, M.-C. Chen, A. Hankla, X. Gao, B. Shim, A. Gaeta, M. Tarazkar, D. Romanov, R. Levis, J. Gaffney, M. Foord, S. Libby, A. Jaron-Becker, A. Becker, L. Plaja, and T. Popmintchev, "Ultraviolet surprise: Efficient soft X-ray high-harmonic generation in multiply ionized plasmas," Science **350**(6265), 1225–1231 (2015).
6. H.-W. Sun, P.-C. Huang, Y.-H. Tzeng, J.-T. Huang, C. D. Lin, C. Jin, and M.-C. Chen, "Extended phase matching of high harmonic generation by plasma-induced defocusing," Optica **4**(8), 976–981 (2017).
7. J. Pupeikis, P. A. Chevreuil, N. Bigler, L. Gallmann, C. R. Phillips, and U. Keller, "Water window soft x-ray source enabled by 25-W few-cycle mid-IR OPCPA at 100 kHz," Optica **7**, 2334–2536 (2019).
8. T. O. Clatterbuck, C. Lyngå, P. M. Paul, L. F. DiMauro, M. B. Gaarde, K. J. Schafer, P. Agostini, K. C. Kulander, and I. Walmsley, "Yield and temporal characterization of high-order harmonics from intense midinfrared excitation of a cesium vapor," Phys. Rev. A **69**(3), 033807 (2004).
9. P. M. Paul, T. O. Clatterbuck, C. Lyngå, P. Colosimo, L. F. DiMauro, P. Agostini, and K. C. Kulander, "Enhanced High Harmonic Generation from an Optically Prepared Excited Medium," Phys. Rev. Lett. **94**(11), 113906 (2005).
10. Y. Akiyama, K. Midorikawa, Y. Matsunawa, Y. Nagata, M. Obara, H. Tashiro, and K. Toyoda, "Generation of high-order harmonics using laser-produced rare-gas-like ions," Phys. Rev. Lett. **69**(15), 2176–2179 (1992).
11. R. Ganeev, M. Suzuki, M. Baba, H. Kuroda, and T. Ozaki, "High-order harmonic generation from boron plasma in the extreme-ultraviolet range," Opt. Lett. **30**(7), 768–770 (2005).
12. S. S. Harilal, B. E. Brumfield, N. L. LaHaye, K. C. Hartig, and M. C. Phillips, "Optical spectroscopy of laser-produced plasmas for standoff isotopic analysis," Appl. Phys. Rev. **5**(2), 021301 (2018).
13. R. A. Ganeev, M. Suzuki, M. Baba, and H. Kuroda, "Generation of strong coherent extreme ultraviolet radiation from the laser plasma produced on the surface of solid targets," Appl. Phys. B **81**(8), 1081–1089 (2005).
14. R. A. Ganeev, L. B. E. Bom, and T. Ozaki, "High-order harmonic generation from plasma plume pumped by 400 nm wavelength laser," Appl. Phys. Lett. **91**(13), 131104–131106 (2007).
15. R. A. Ganeev, L. B. E. Bom, T. Ozaki, and P. V. Redkin, "Maximizing the yield and cutoff of high-order harmonic generation from plasma plume," J. Opt. Soc. Am. B **24**(11), 2770–2778 (2007).
16. R. A. Ganeev, H. Singhal, P. A. Naik, U. Chakravarty, V. Arora, J. A. Chakera, R. A. Khan, M. Raghuramaiah, S. R. Kumbhare, R. P. Kushwaha, and P. D. Gupta, "Optimization of the high-order harmonics generated from silver plasma," Appl. Phys. B **87**(2), 243–247 (2007).
17. R. A. Ganeev, M. Suzuki, and H. Kuroda, "Quasi-phase-matching of high-order harmonics in multiple plasma jets," Phys. Rev. A **89**(3), 033821 (2014).
18. R. A. Ganeev, M. Suzuki, and H. Kuroda, "Advanced properties of extended plasmas for efficient high-order harmonic generation," Phys. Plasmas **21**(5), 053503 (2014).
19. C. Hutchison, R. A. Ganeev, T. Witting, F. Frank, W. A. Okell, J. W. G. Tisch, and J. P. Marangos, "Stable generation of high-order harmonics of femtosecond laser radiation from laser produced plasma plumes at 1 kHz pulse repetition rate," Opt. Lett. **37**(11), 2064–2066 (2012).
20. R. A. Ganeev, L. B. E. Bom, J. C. Kieffer, M. Suzuki, H. Kuroda, and T. Ozaki, "Demonstration of the 101st harmonic generated from a laser-produced manganese plasma," Phys. Rev. A **76**(2), 023831 (2007).
21. M. Suzuki, M. Baba, R. Ganeev, H. Kuroda, and T. Ozaki, "Anomalous enhancement of a single high-order harmonic by using a laser-ablation tin plume at 47 nm," Opt. Lett. **31**(22), 3306–3308 (2006).
22. M. Suzuki, R. A. Ganeev, L. B. E. Bom, M. Baba, T. Ozaki, and H. Kuroda, "Extension of cutoff in high harmonic by using doubly charged ions in a laser-ablation plume," J. Opt. Soc. Am. B **24**(11), 2847–2852 (2007).
23. M. Singh, M. A. Fareed, V. Strelkov, A. N. Grum-Grzhimailo, A. Magunov, A. Laramée, F. Légaré, and T. Ozaki, "Intense quasi-monochromatic resonant harmonic generation in the multiphoton ionization regime," Optica **8**(8), 1122–1125 (2021).
24. E. Constant, D. Garzella, P. Breger, E. Mével, C. Dorrer, C. Le Blanc, F. Salin, and P. Agostini, "Optimizing High Harmonic Generation in Absorbing Gases: Model and Experiment," Phys. Rev. Lett. **82**(8), 1668–1671 (1999).
25. E. L. Falcão-Filho, C.-J. Lai, K.-H. Hong, V.-M. Gkortsas, S.-W. Huang, L.-J. Chen, and F. X. Kärtner, "Scaling of high-order harmonic efficiencies with visible wavelength drivers: A route to efficient extreme ultraviolet sources," Appl. Phys. Lett. **97**(6), 061107 (2010).
26. J. Rothhardt, S. Hädrich, S. Demmler, M. Krebs, S. Fritzsche, J. Limpert, and A. Tünnermann, "Enhancing the Macroscopic Yield of Narrow-Band High-Order Harmonic Generation by Fano Resonances," Phys. Rev. Lett. **112**(23), 233002 (2014).
27. H. Wang, Y. Xu, S. Ulonska, J. S. Robinson, P. Ranitovic, and R. A. Kaindl, "Bright high-repetition-rate source of narrowband extreme-ultraviolet harmonics beyond 22 eV," Nat. Commun. **6**(1), 7459–7465 (2015).

Optics EXPRESS

28. H. Singhal, V. Arora, B. S. Rao, P. A. Naik, U. Chakravarty, R. A. Khan, and P. D. Gupta, "Dependence of high-order harmonic intensity on the length of preformed plasma plumes," Phys. Rev. A **79**(2), 023807 (2009).
29. N. Rosenthal and G. Marcus, "Discriminating between the Role of Phase Matching and that of the Single-Atom Response in Resonance Plasma-Plume High-Order Harmonic Generation," Phys. Rev. Lett. **115**(13), 133901 (2015).
30. A. L'Huillier, X. F. Li, and L. A. Lompré, "Propagation effects in high-order harmonic generation in rare gases," J. Opt. Soc. Am. B **7**(4), 527–536 (1990).
31. C. G. Durfee, A. R. Rundquist, S. Backus, C. Herne, M. M. Murnane, and H. C. Kapteyn, "Phase Matching of High-Order Harmonics in Hollow Waveguides," Phys. Rev. Lett. **83**(11), 2187–2190 (1999).
32. R. A. Ganeev, P. A. Naik, H. Singhal, J. A. Chakera, and P. D. Gupta, "Strong enhancement and extinction of single harmonic intensity in the mid- and end-plateau regions of the high harmonics generated in weakly excited laser plasmas," Opt. Lett. **32**(1), 65–67 (2007).
33. V. V. Kim, G. S. Boltaev, M. Iqbal, N. A. Abbasi, H. Al-Harmi, I. S. Wahyutama, T. Sato, K. L. Ishikawa, R. A. Ganeev, and A. S. Alnaser, "Resonance enhancement of harmonics in the vicinity of 32 nm spectral range during propagation of femtosecond pulses through the molybdenum plasma," J. Phys. B: At. Mol. Opt. Phys. **53**(19), 195401 (2020).
34. W. Fu, Y. H. Lai, J. Liang, and W. Li, "Investigation of high-harmonic cutoff of metal ions driven by near-infrared laser," Opt. Express **30**(13), 23090–23101 (2022).
35. E. Gamaly, A. Rode, and B. Luther-Davies, "Ultrafast Ablation with High-Pulse-Rate Lasers. Part I: Theoretical Considerations," J. Appl. Phys. **85**(8), 4213–4221 (1999).
36. E. G. Gamaly, A. V. Rode, B. Luther-Davies, and V. T. Tikhonchuk, "Ablation of solids by femtosecond lasers: Ablation mechanism and ablation thresholds for metals and dielectrics," Phys. Plasmas **9**(3), 949–957 (2002).